DOI: 10.13009/EUCASS2019-674

Research of Hypersonic Boundary Layer Instability with Thermal-Chemical Non-equilibrium Effects

Xianliang Chen⋆ *and Song Fu*⋆†
⋆*School of Aerospace Engineering, Tsinghua University, Beijing, 100084, China*
chenxl0728@163.com · fs-dem@tsinghua.edu.cn
†Corresponding author

Abstract

As the Mach number increases in hypersonic flows, thermal-chemical nonequilibrium effects gradually occur and inevitably influence the boundary layer stability and transition process. In this work, the instability behaviour of thermal-chemical nonequilibrium flows are studied by using linear stability theory and parabolized stability equation in the range of Mach number smaller than 10. The reliability of the developed solver is examined and the destabilizing effect of thermal-chemical nonequilibrium is compared.

1. Introduction

Hypersonic boundary layer instability and transition have recently become a focal topic of research in aeronautics. The outline provided by Morkovin et al[23] in Figure 1 shows five different transition paths according to the level of disturbance. The path (a) with minimum disturbance is known as the natural transition, where disturbances are excited through receptivity mechanisms, experience linear modal growth downstream and breakdown to turbulence through nonlinear interactions. To explore the physical mechanisms of the process, stability theories and the corresponding numerical methods have been persistently developed on relatively solid mathematical foundations, such as the quasi-parallel normal-mode instability,[18,26] the parabolized stability equation (PSE)[2,5] suitable for non-parallelism and nonlinearity, and the most complete yet resource-consuming direct numerical simulation (DNS).[16,20]

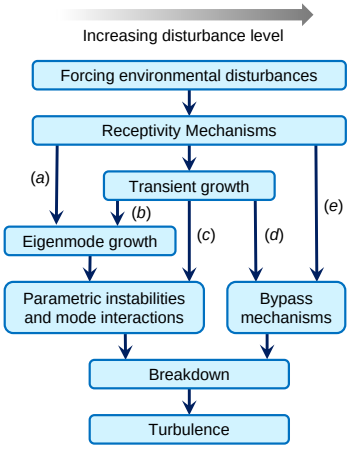

Figure 1: Transition paths to turbulence in boundary layer flow.[8,23]

Meanwhile, an important feature of hypersonic flow is the steeply-rising temperature within the field. As shown in Figure 2, extremely high temperatures excite vibrational energy within molecules and cause chemical dissociation and even ionization, which in turn decreases the temperature and fails the ideal gas assumption.[1] Thermal-chemical equilibrium models were firstly developed and applied to hypersonic flow simulations.[28,29] However, as the rates of thermal and chemical process are physically finite, nonequilibrium models were subsequently developed,[10] which increased the simulation reliability as well as the computational cost. As a consequence, the effects of thermal-chemical nonequilibrium on stability and transition is a question to answer.

DOI: 10.13009/EUCASS2019-674

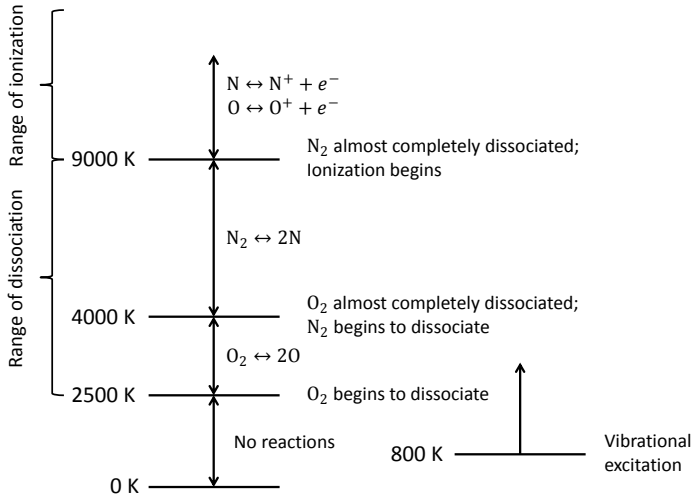

Figure 2: Temperature ranges for different thermal-chemical process.[1]

Malik & Anderson[19] pioneered the research of real-gas effects on boundary layer instability by comparing equilibrium gas with ideal gas, and found that for Mach 10 plate real-gas effects not only destabilized the second mode but also decreased the second mode frequency, different from the earlier belief that anything that thins the boundary layer should increase the frequency. Bitter[3] performed a detailed research on thermal nonequilibrium gas instability up to Mach 5, and provided scaling results of the second mode and estimations of vibrational effects. Meanwhile, Chang & Malik[6] developed the PSE solver with thermal-chemical nonequilibrium effects and presented abundant results on the e^N predictions of hypersonic flight transition, showing the applicability of linear stability theories on hypersonic flows. However, nonlinear interactions and the role that nonlinearity plays in the transition prediction were neglected, indicating the demand of nonequilibrium nonlinear PSE solver. DNS is an answer to the far downstream nonlinear process, yet the current DNS results concerning thermal-chemical nonequilibrium effects, for example from the Zhong's group,[13,17,24] are mainly on receptivity and linear normal-mode instability.

The flow considered in this paper is a flat plate in the range of Mach number smaller than 10. Ionization is neglected because the highest temperature for adiabatic wall is less than 6000K. For initial composition of air being N_2 and O_2, a classic five-species mixture (N_2, O_2, NO, N, O) is chosen.

2. Physical models and numerical methods

2.1 Governing equations

To describe the thermal-chemical nonequilibrium gases, additional conservations of vibrational energy and species mass are coupled into the Navier-Stokes equation. The non-dimensional equations are written as follows:

$$\frac{\partial \rho}{\partial t} + \nabla \cdot (\rho \boldsymbol{U}) = 0 \tag{1a}$$

$$\rho \frac{\mathrm{D}\boldsymbol{U}}{\mathrm{D}t} + \nabla p = \frac{1}{Re_L} \nabla \cdot \boldsymbol{\tau} \tag{1b}$$

$$\rho c_{p,tr} \frac{\mathrm{D}T}{\mathrm{D}t} - Ec \frac{\mathrm{D}p}{\mathrm{D}t} = \frac{Ec}{Re_L} (\boldsymbol{\tau} : \nabla \boldsymbol{U}) + \nabla \cdot \left(\frac{k_{tr}}{Re_L} \nabla T \right) + \frac{\mu}{Re_L Sc} \nabla T \cdot \left(\sum_{s=1}^{n_s} c_{ptr,s} \nabla Y_s \right) - Re_L \left(Q_{t-v} + \sum_{s=1}^{n_s} h_s \dot{\omega}_s \right) \tag{1c}$$

$$\rho c_{vib} \frac{\mathrm{D}T_v}{\mathrm{D}t} = \nabla \cdot \left(\frac{k_v}{Re_L} \nabla T_v \right) + \frac{\mu}{Re_L Sc} \nabla T_v \cdot \left(\sum_{s=1}^{n_v} c_{vib,s} \nabla Y_s \right) + Re_L Q_{t-v} \tag{1d}$$

$$\rho \frac{\mathrm{D}Y_s}{\mathrm{D}t} = \nabla \cdot \left(\frac{\mu}{Re_L Sc} \nabla Y_s \right) + Re_L \dot{\omega}_s \tag{1e}$$

DOI: 10.13009/EUCASS2019-674

$$p = \rho T \sum_{s=1}^{n_s} R_s Y_s \tag{1f}$$

with dimensionless quantities defined as:

$$\begin{cases} \boldsymbol{x} = \dfrac{\boldsymbol{x}^*}{L^*}, \quad t = \dfrac{t^* U_\infty^*}{L^*}, \quad \boldsymbol{U} = \dfrac{\boldsymbol{U}^*}{U_\infty^*}, \quad \rho = \dfrac{\rho^*}{\rho_\infty^*}, \quad p = \dfrac{p^*}{\rho_\infty^* U_\infty^{*2}}, \quad T = \dfrac{T^*}{T_\infty^*}, \quad T_v = \dfrac{T_v^*}{T_\infty^*} \\ c_{p,tr} = \dfrac{c_{p,tr}^*}{c_{ptr,\infty}^*}, \quad c_{vib} = \dfrac{c_{vib}^*}{c_{ptr,\infty}^*}, \quad h_s = \dfrac{h_s^*}{c_{ptr,\infty}^* T_\infty^*}, \quad e_{vib} = \dfrac{e_{vib}^*}{c_{ptr,\infty}^* T_\infty^*}, \quad Ec = \dfrac{U_\infty^{*2}}{c_{ptr,\infty}^* T_\infty^*} = (\gamma_\infty - 1) Ma^2 \\ \mu = \dfrac{\mu^*}{\mu_\infty^*}, \quad k_{tr} = \dfrac{k_{tr}^*}{\mu_\infty^* c_{ptr,\infty}^*}, \quad k_v = \dfrac{k_v^*}{\mu_\infty^* c_{ptr,\infty}^*}, \quad Sc = \dfrac{\mu}{\rho D_s}, \quad Q_{t-v} = \dfrac{Q_{t-v}^* \mu_\infty^*}{\rho_\infty^{*2} U_\infty^{*2} c_{ptr,\infty}^* T_\infty^*}, \quad \dot{\omega}_s = \dfrac{\dot{\omega}_s^* \mu_\infty^*}{\rho_\infty^{*2} U_\infty^{*2}}. \end{cases} \tag{2}$$

Asterisks and ∞ signify dimensional and freestream quantities. s denotes the s-th species with n_s and n_v the numbers of species and diatomic species. Variables T^* and T_v^* are the translational/rotational (TR) temperature and vibrational temperature; $Y_s = \rho_s^*/\rho^*$ is the mass fraction; h^* is the specific enthalpy with c_{ptr}^* and c_{vib}^* the TR and vibrational specific heat; γ is the specific heat ratio; Re_L is the Reynolds number on reference length scale L^*. The source terms Q_{t-v}^* and $\dot{\omega}_s^*$ are introduced for the translation-vibrational energy exchange[21] and the finite-rate reactions.[25] The calculation of transport parameters (viscosity μ^*, conductivity k^* and mass-diffusion coefficients D_s^*) employs Blottner's curve fit[4] and Wilke's mixing rule.[30] Details can be found in Hudson.[12] As a comparison, a new unified curve-fit is provided in the range of (120~10000 K) based on Gupta et al[11] and Cole & Wakeham:[7]

$$\mu_s^* = 0.1 \exp\left[A_{1s}(\ln T^*)^3 + A_{2s}(\ln T^*)^2 + A_{3s} \ln T^* + A_{4s}\right] \tag{3}$$

as the Blottner's curves overestimate viscosity in the room-temperature range.

More concisely, (1) is expressed as:

$$\mathscr{L}(\boldsymbol{Q}) = 0 \tag{4}$$

where $\boldsymbol{Q} = [\rho, U, V, W, T, T_v, Y_s]^{\mathrm{T}}$, $s \in [2, n_s]$. For stability analysis, $\boldsymbol{Q}$ is divided into a steady part $\bar{\boldsymbol{Q}}$ and a disturbance part $\boldsymbol{q}$. These two parts are solved separately.

$$\boldsymbol{Q}(x, y, z, t) = \bar{\boldsymbol{Q}}(x, y, z) + \boldsymbol{q}(x, y, z, t), \qquad \begin{cases} \bar{\boldsymbol{Q}} = \left[\bar{\rho}, \bar{U}, \bar{V}, \bar{W}, \bar{T}, \bar{T}_v, \bar{Y}_s\right]^{\mathrm{T}} \\ \boldsymbol{q} = [\sigma, u, v, w, \theta, \theta_v, y_s]^{\mathrm{T}} \end{cases} \quad s \in [2, n_s] \tag{5}$$

2.2 Calculation of basic flow

The flow treated here is a flat-plate boundary layer with zero angle of attack. The steady basic flow is obtained either by the unsteady Navier-Stokes (NS) solver, or by the parabolized boundary layer equation (BLE) solver.

The unsteady thermal-chemical nonequilibrium NS solver employs finite-volume scheme. The inviscid flux terms are discretized using Roe's scheme,[15,27] with left and right states reconstructed by 2nd order MUSCL scheme.[14] Fully implicit LUSGS method is implemented as the time-stepping method for quick convergence.[31,32]

As the NS solver is time-consuming, the boundary layer assumption is introduced and the equation is then parabolized if the effect of head shock is neglected downstream. As the edge of the boundary layer is assumed to be uniform, the dimensionless Lees-Dorodnitsyn transformation is employed to remove the singularity at origin:

$$\eta(x, y) = \sqrt{\frac{Re_L}{x}} \int_0^y \rho \mathrm{d}y \tag{6}$$

Because of the existence of non-equilibrium source terms, the boundary layer is no longer self-similar. Instead, an efficient streamwise-marching procedure is implemented.[4] Chebyshev collocation-point and 3rd order finite difference are used in the η and x direction, respectively. Newtonian implicit iteration is employed for 2nd order convergence.

DOI: 10.13009/EUCASS2019-674

2.3 Calculation of disturbance

The governing equation for disturbance is derived through:

$$\mathscr{L}\left(\bar{\boldsymbol{Q}}+\boldsymbol{q}\right)-\mathscr{L}\left(\bar{\boldsymbol{Q}}\right)=0 \tag{7}$$

The above equation is expanded and rewritten into a compact matrix form:

$$\boldsymbol{F}\frac{\partial \boldsymbol{q}}{\partial t}+\boldsymbol{A}\frac{\partial \boldsymbol{q}}{\partial x}+\boldsymbol{B}\frac{\partial \boldsymbol{q}}{\partial y}+\boldsymbol{C}\frac{\partial \boldsymbol{q}}{\partial z}+\boldsymbol{D}\boldsymbol{q}=\boldsymbol{H}_{xx}\frac{\partial^2 \boldsymbol{q}}{\partial x^2}+\boldsymbol{H}_{yy}\frac{\partial^2 \boldsymbol{q}}{\partial y^2}+\boldsymbol{H}_{zz}\frac{\partial^2 \boldsymbol{q}}{\partial z^2}+\boldsymbol{H}_{xy}\frac{\partial^2 \boldsymbol{q}}{\partial x\partial y}+\boldsymbol{H}_{yz}\frac{\partial^2 \boldsymbol{q}}{\partial y\partial z}+\boldsymbol{H}_{zx}\frac{\partial^2 \boldsymbol{q}}{\partial z\partial x}+\boldsymbol{N} \tag{8}$$

where $\boldsymbol{F}$, $\boldsymbol{A}$, $\boldsymbol{B}$, $\boldsymbol{C}$, $\boldsymbol{D}$ and $\boldsymbol{H}$ are 10×10 matrices and only related to the basic flow. $\boldsymbol{N}$ represents non-linear terms.

We follow the PSE formulation procedures proposed by Chang & Malik.[5] Briefly speaking, the disturbance is assumed to be periodic in time and in the spanwise direction, so the total disturbance is expressed as Fourier series:

$$\boldsymbol{Q}\left(x,y,z,t\right)=\bar{\boldsymbol{Q}}\left(x,y\right)+\sum_{m=-M}^{M}\sum_{n=-N}^{N}\hat{\boldsymbol{q}}_{mn}\left(x,y\right)\exp\left[\mathrm{i}\left(\int_{x_0}^{x}\alpha_{mn}\mathrm{d}x+n\beta z-m\omega t\right)\right] \tag{9}$$

where ω and β are the pre-specified minimum frequency and spanwise wavenumber. α_{mn} and $\hat{\boldsymbol{q}}_{mn}$ are the Fourier components of the streamwise wave number and shape function for the mode (m,n). M and N denote the truncated modes. The shape function is discretized using 4^{th} order central difference scheme. The streamwise marching employs 2^{nd} or 1^{st} order backward difference. The wavenumber at each station is updated as:

$$\alpha^{\text{new}}=\alpha^{\text{old}}-\mathrm{i}\frac{\displaystyle\int_0^{\infty}\bar{\rho}\left(u^{\dagger}\frac{\partial u}{\partial x}+v^{\dagger}\frac{\partial v}{\partial x}+w^{\dagger}\frac{\partial w}{\partial x}\right)\mathrm{d}y}{\displaystyle\int_0^{\infty}\bar{\rho}\left(u^{\dagger}u+v^{\dagger}v+w^{\dagger}w\right)\mathrm{d}y} \tag{10}$$

where † denotes complex conjugate. Owing to the high frequency disturbance, the boundary conditions employed for shape functions are:

$$\begin{cases}\hat{u}_{mn}=\hat{v}_{mn}=\hat{w}_{mn}=\hat{\theta}_{mn}=\hat{\theta}_{v,mn}=\dfrac{\partial \hat{y}_{s,mn}}{\partial y}=0, & y=0\\ \hat{u}_{mn},\ \hat{v}_{mn},\ \hat{w}_{mn},\ \hat{\theta}_{mn},\ \hat{\theta}_{v,mn},\ \hat{y}_{s,mn}=0, & y\to\infty\end{cases} \tag{11}$$

In terms of modal instability, the variation of α_{mn} and $\hat{\boldsymbol{q}}_{mn}$ in the streamwise direction is neglected and the nonlinear terms are dropped:

$$\boldsymbol{Q}\left(x,y,z,t\right)=\bar{\boldsymbol{Q}}\left(y\right)+\mathrm{Re}\{\hat{\boldsymbol{q}}\left(y\right)\exp\left[\mathrm{i}\left(\alpha x+\beta z-\omega t\right)\right]\} \tag{12}$$

The above equation leads to an eigenvalue problem.

A commonly used length scale in a boundary layer is $\delta^*=\left(\nu_{\infty}^* x^*/U_{\infty}^*\right)^{1/2}$ and the corresponding Reynolds number is $Re=\sqrt{Re_x}$, where ν^* is the kinetic viscosity. Dimensionless frequency is expressed as $F=\omega/Re$, and phase velocity $c_r=\omega/\mathrm{Re}\left(\alpha\right)$ is defined to describe the propagating speed of disturbance.

3. Results and discussion

Firstly, the reliability of modal-instability solver and thermal-chemical models is examined, as shown in Figure 3 and 4. The case of Figure 3a is a Ma 5.5 flat plate for ideal gas obtained from Fedorov[9] ($T_{\infty}^*=70\,\mathrm{K}$, $T_w/T_{\text{ad}}=0.1$ and $F=10^{-4}$). The case of Figure 3b is a Ma 10 flat plate for chemically-nonequilibrium gas obtained from Miró[22] ($Re_{\infty}=6.6\times10^6$ /m, $T_{\infty}^*=600\,\mathrm{K}$, adiabatic wall and $x^*=0.6\,\mathrm{m}$). The case of 4 is a Ma 4.5 flat plate for thermal-nonequilibrium gas obtained from Bitter[3] ($T_{\infty}^*=1500\,\mathrm{K}$, $p_{\infty}^*=10$ kPa, $T_w^*=300\,\mathrm{K}$, $Re=2000$). All present results show good agreements with literatures.

Afterwards, the PSE solver is verified in terms of both linear and nonlinear cases. The linear PSE solver is compared with Ma & Zhong's DNS results on Ma 4.5 flat plate receptivity[16] ($T_{\infty}^*=65.15\,\mathrm{K}$, adiabatic wall and $F=2.2\times10^{-4}$). The basic flow is obtained from NS solver and the growth rate from PSE fits remarkably well with DNS, as shown in Figure 5a, showing the great capability of PSE on the prediction of linear growth. By contrast, quasi-parallel LST underestimates the growth rate though employing the same basic flow, indicating the significance of non-parallelism effect. In Figure 5b, the nonlinear PSE solver is examined through the classic Ma 1.6 oblique breakdown case analyzed by Chang & Malik[5] ($T_{\infty}^*=300\,\mathrm{K}$, adiabatic wall, $F=0.2\times10^{-4}$, $\beta/Re=0.83\times10^{-4}$ and $u_{\max}^{(1,1)}=0.1\%$). The NPSE is capable of predicting the weakly nonlinear interactions of disturbances until the onset of transition downstream, and is expected to play a more important role in the research of nonequilibrium hypersonic boundary layer transition.

DOI: 10.13009/EUCASS2019-674

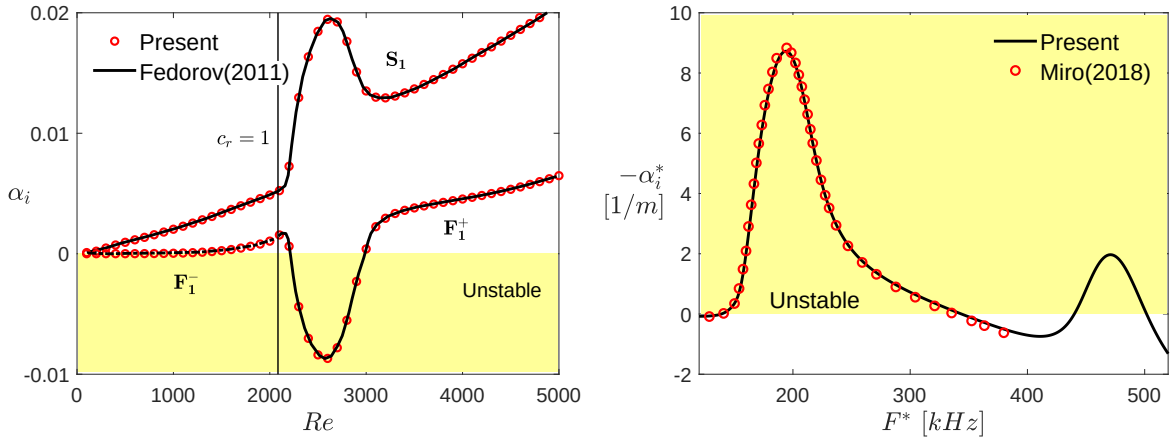

(a) Ma 5.5 flat-plate case

(b) Ma 10 flat-plate case

Figure 3: Comparison of the modal growth rate between present solver and literatures.

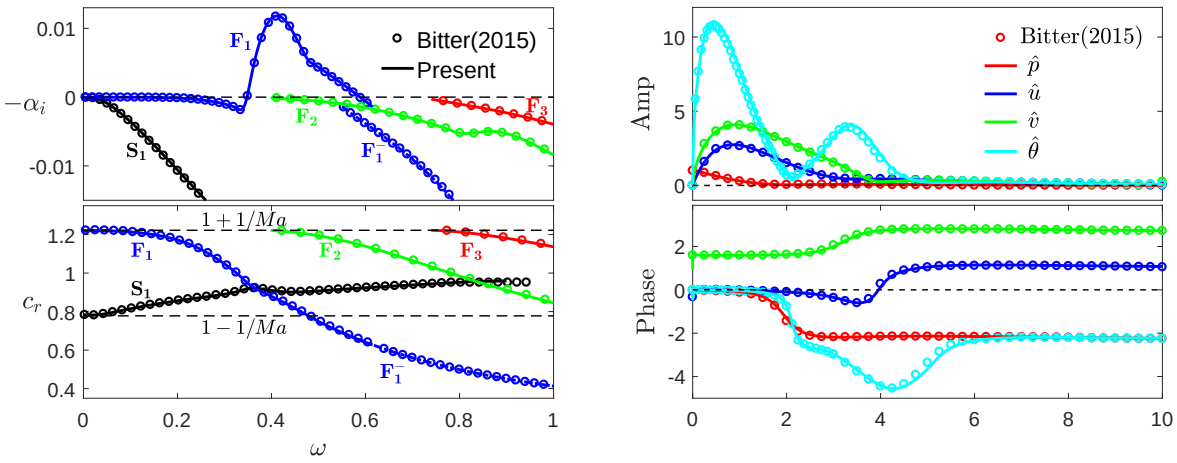

(a) Growth rate and phase velocity,

(b) Shape function and phase angle of the second mode

Figure 4: Comparison of the modal instability between present solver and literatures, Ma 4.5 flat-plate case

4. Acknowledgments

This work is supported by NSFC Grant 11572176.

References

[1] J. D. Anderson. *Hypersonic and High-Temperature Gas Dynamics, Second Edition*. McGraw-Hill, 2006.

[2] F. P. Bertolotti, T. Herbert, and P. R. Spalart. Linear and nonlinear stability of the blasius boundary layer. *Journal of Fluid Mechanics*, 242(9):441–474, 1992.

[3] N. P. Bitter and J. E. Shepherd. Stability of highly cooled hypervelocity boundaryălayers. *Journal of Fluid Mechanics*, 778:586–620, 2015.

[4] F. G. Blottner. Chemical nonequilibrium boundary layer. *Journal of Spacecraft & Rockets*, 40(5):810–818, 1963.

[5] C.-L. Chang and M. R. Malik. Oblique-mode breakdown and secondary instability in supersonic boundary layers. *Journal of Fluid Mechanics*, 273:323–360, 1994.

DOI: 10.13009/EUCASS2019-674

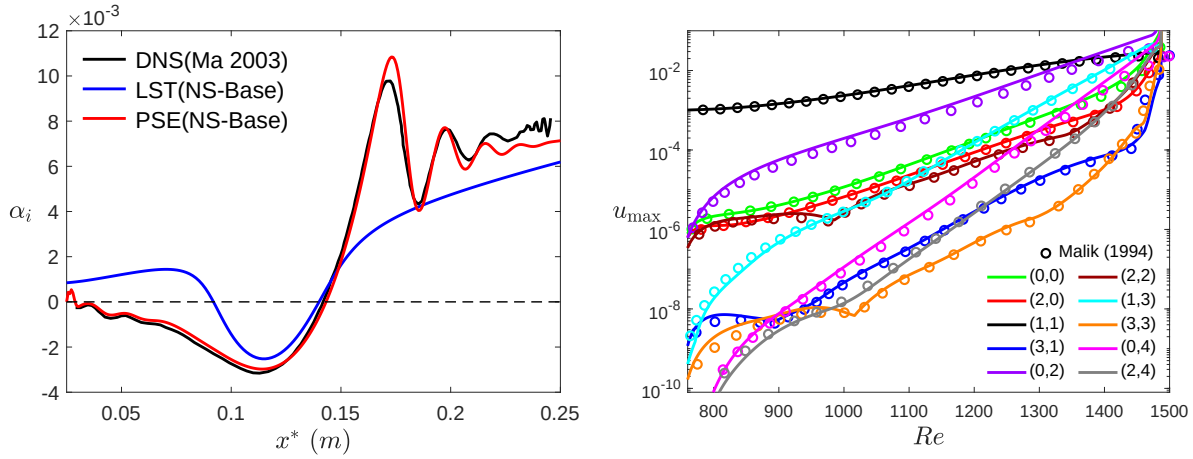

(a) Linear growth, Ma 4.5 flat-plate case

(b) Nonlinear growth, Ma 1.6 case flat-plate

Figure 5: Comparision of the linear/nonlinear growth between present solver and literatures.

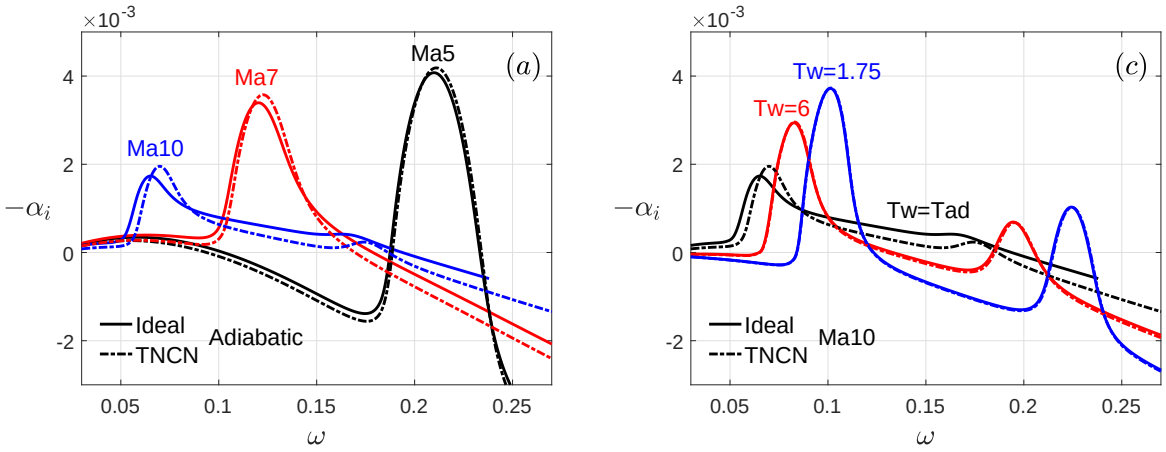

(a) Linear growth, Ma 4.5 flat-plate case

(b) Nonlinear growth, Ma 1.6 case flat-plate

Figure 6: Comparision of the linear/nonlinear growth between present solver and literatures.

[6] C.-L. Chang and M. R. Malik. Hypersonic boundary-layer stability with chemical reactions using pse. In *Fluid Dynamics Conference*, 1997.

[7] W. A. Cole and W. A. Wakeham. The viscosity of nitrogen, oxygen, and their binary mixtures in the limit of zero density. *Journal of Physical & Chemical Reference Data*, 14(1):209–226, 1985.

[8] A. Fedorov. Transition and stability of high-speed boundary layers. *Annual Review of Fluid Mechanics*, 43(1):79–95, 2011.

[9] A. Fedorov and A. Tumin. High-speed boundary-layer instability: Old terminology and a new framework. *AIAA Journal*, 49(8):1647–1657, 2011.

[10] Peter A. Gnoffo, Roop N. Gupta, and J L Shinn. Conservation equations and physical models for hypersonic air flows in thermal and chemical nonequilibrium. Report, NASA Langley Research Center, 1989.

[11] Roop N. Gupta, Jerrold M. Yos, and Richard A. Thompson. A review of reaction rates and thermodynamic and transport properties for the 11-species air model for chemical and thermal nonequilibrium calculations to 30000 K. Report, Scientific Research and Technology, Inc., 1990.

[12] M. L. Hudson. *Linear Stability of Hypersonic Flows in Thermal and Chemical Nonequilibrium*. Thesis, North Carolina State University, 1996.

DOI: 10.13009/EUCASS2019-674

[13] C. P. Knisely and Zhong X. L. Significant supersonic modes and the wall temperature effect in hypersonic boundary layers. *AIAA Journal*, 57(4):1552–1566, 2019.

[14] B. V. Leer. Towards the ultimate conservative difference scheme. v - a second-order sequel to godunov's method. *Journal of Computational Physics*, 32(1):101–136, 1979.

[15] Y. Liu and M. Vinokur. Nonequilibrium flow computations. i. an analysis of numerical formulations of conservation laws. *Journal of Computational Physics*, 83(2):373–397, 1988.

[16] Y. Ma and X. Zhong. Receptivity of a supersonic boundary layer over a flat plate. part 1. wave structures and interactions. *Journal of Fluid Mechanics*, 488(488):31–78, 2003.

[17] Y. Ma and X. Zhong. Receptivity to freestream disturbances of a Mach 10 nonequilibrium reacting oxygen flow over a flat plate. *AIAA Journal*, 2004.

[18] L. M. Mack. Boundary-layer linear stability theory. In *AGARD Special Course on Stability and Transition of Laminar Flow*, page 81, 1984.

[19] M. R. Malik and E. C. Anderson. Real gas effects on hypersonic boundarylayer stability. *Physics of Fluids*, 3(5):803–821, 1991.

[20] C. S. J. Mayer, D. A. Von Terzi, and H. F. Fasel. Direct numerical simulation of complete transition to turbulence via oblique breakdown at mach 3. *Journal of Fluid Mechanics*, 674:5–42, 2011.

[21] R. C. Millikan and D. R. White. Systematics of vibrational relaxation. *Journal of Chemical Physics*, 39(12):3209–3213, 1963.

[22] F. M. Miró, F. Pinna, E. S. Beyak, P. Barbante, and H. L. Reed. Diffusion and chemical non-equilibrium effects on hypersonic boundary-layer stability. In *AIAA Aerospace Sciences Meeting*, 2018.

[23] M. V. Morkovin, E. Reshotko, and T. Herbert. Transition in open flow systems-a reassessment. *Bull. APS*, 39(9):1–31, 1994.

[24] C. H. Mortensen and X. Zhong. Simulation of second-mode instability in a real-gas hypersonic flow with graphite ablation. *AIAA Journal*, 52(8):1632–1652, 2015.

[25] C. Park, R. L. Jaffe, and H. Partridge. Chemical-kinetic parameters of hyperbolic earth entry. *Journal of Thermophysics and Heat Transfer*, 15(1):76–90, 2001.

[26] H. L. Reed, W. S. Saric, and D. Arnal. Linear stability theory applied to boundary layers. *Annual Review of Fluid Mechanics*, 28(1):389–428, 1996.

[27] P. L. Roe. Approximate riemann solvers, parameter vectors, and difference schemes. *Journal of computational physics*, pages 357–372, 1981.

[28] S. Srinivasan and J. C. Tannehill. Simplified curve fits for the transport properties of equilibrium air. Report, Iowa State University, 1987.

[29] J. C. Tannehill and P. H. Mugge. Improved curve fits for the thermodynamic properties of equilibrium air suitable for numerical computation using time-dependent or shock-capturing methods. *NASA Contractor Report*, 1974.

[30] C. R. Wilke. A viscosity equation for gas mixtures. *Journal of Chemical Physics*, 18(4):517–519, 1950.

[31] S. Yoon and D. Kwak. Artificial dissipation models for hypersonic external flow. *AIAA Journal*, 1988.

[32] S. T. Yu, Y. L. P. Tsai, and J. S. Shuen. Three-dimensional calculations of supersonic reacting flows using an lu scheme. *Journal of Computational Physics*, 101(2):276–286, 1992.